



Ries and Chicxulub: Impact craters on Earth provide insights for Martian ejecta blankets

T. KENKMANN* and F. SCHÖNIAN

Institut für Mineralogie, Museum für Naturkunde, Humboldt-Universität Berlin, Invalidenstrasse 43, D-10115 Berlin, Germany

*Corresponding author. E-mail: thomas.kenkmann@museum.hu-berlin.de

(Received 15 October 2005; revision accepted 24 April 2006)

Abstract—Terrestrial impact structures provide field evidence for cratering processes on planetary bodies that have an atmosphere and volatiles in the target rocks. Here we discuss two examples that may yield implications for Martian craters:

1. Recent field analysis of the Ries crater has revealed the existence of subhorizontal shear planes (detachments) in the periphery of the crater beneath the ejecta blanket at 0.9–1.8 crater radii distance. Their formation and associated radial outward shearing was caused by weak spallation and subsequent dragging during deposition of the ejecta curtain. Both processes are enhanced in rheologically layered targets and in the presence of fluids. Detachment faulting may also occur in the periphery of Martian impacts and could be responsible for the formation of lobe-parallel ridges and furrows in the inner layer of double-layer and multiple-layer ejecta craters.
2. The ejecta blanket of the Chicxulub crater was identified on the southeastern Yucatán Peninsula at distances of 3.0–5.0 crater radii from the impact center. Abundance of glide planes within the ejecta and particle abrasion both rise with crater distance, which implies a ground-hugging, erosive, and cohesive secondary ejecta flow. Systematic measurement of motion indicators revealed that the flow was deviated by a preexisting karst relief. In analogy with Martian fluidized ejecta blankets, it is suggested that the large runout was related to subsurface volatiles and the presence of basal glide planes, and was influenced by eroded bedrock lithologies. It is proposed that ramparts may result from enhanced shear localization and a stacking of ejecta material along internal glide planes at decreasing flow rates when the flow begins to freeze below a certain yield stress.

INTRODUCTION

Martian impact craters reveal morphological characteristics such as fluidized ejecta with ramparts that differ from those of other planetary bodies. Ejecta morphologies such as single-layer ejecta, double-layer ejecta, and multiple-layer ejecta (Barlow et al. 2000) depend on crater size, geographic location, altitude, terrain, and time of formation (Mouginis-Mark 1979; Costard 1989; Barlow and Bradley 1990; Barlow 2005; Reiss et al. 2005). These characteristics have been explained by models that emphasize the role of either subsurface ice and water (“subsurface volatile model”) (Carr et al. 1977; Wohletz and Sheridan 1983; Mouginis-Mark 1987; Clifford 1993) or atmospheric turbulence during the cratering process (“ring vortex model”) (Schultz and Gault 1979; Schultz 1992; Barnouin-Jha and Schultz 1996, 1998). The existence of a critical and latitude-dependent onset diameter for which fluidized layered ejecta

occur suggests that subsurface volatiles play a dominant role in the fluidization of ejecta blankets. The relationship between the ejecta type and the subsurface water/ice content and its variation with depth (Wohletz and Sheridan 1983; Mouginis-Mark 1987; Costard 1989; Barlow and Bradley 1990) is currently debated. It critically depends on the rheology of ice and water-bearing rocks and their behavior under shock (Stewart and Ahrens 2003; Ivanov 2005; Ivanov et al. 2005).

On Earth, impact craters also formed in the presence of an atmosphere and subsurface volatiles. This analogy underscores the significance of comparative crater studies, all the more so as the analysis of craters on Mars and Earth yields complementary information on the cratering process. Most of our knowledge of Martian craters is derived from remote sensing data. In contrast, analyses of terrestrial craters comprise a wide spectra of techniques whose applications benefit from easy accessibility and the opportunity of direct

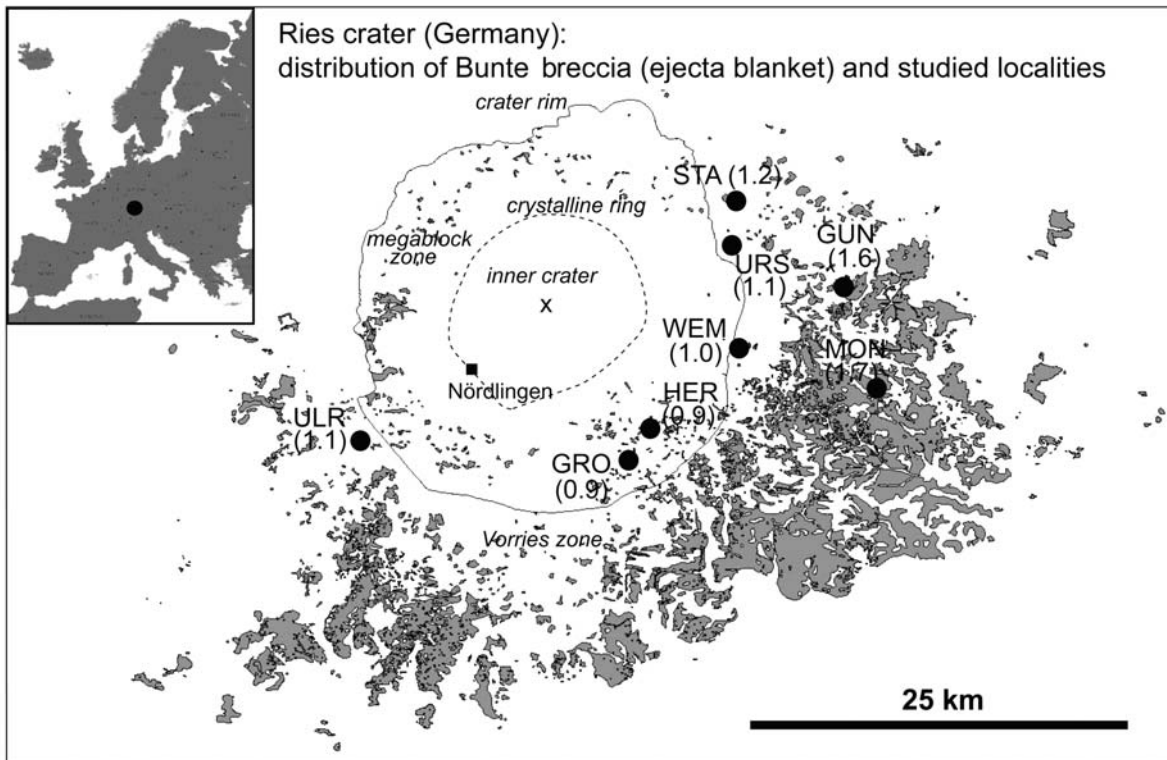


Fig. 1. A simplified map of the Ries crater, southern Germany, showing the principal outline, distribution of Bunte breccia, and studied localities that display detachment horizons. Abbreviations: STA = Stahlmühle, URS = Ursheim E, GUN = Gundelsheim, WEM = Wemding, MON = Monheim, HER = Heroldingen, GRO = Grosssorheim E, ULR = Ulrichsruhe.

sampling of various impact formations. Despite this advantage on Earth, rapid weathering and erosion are likely to destroy delicate features of surface-like ejecta blankets, which, consequently, have relatively short lifetimes. Preservation usually occurs only if the ejecta is rapidly buried by subsequent sediments. This paper reports on recent investigations in two large terrestrial impact structures, Ries and Chicxulub, that belong to the group of rare craters with partly preserved ejecta blankets. These studies may have implications for the role of atmosphere and volatiles in the impact cratering process on Mars.

The Ries crater, Germany, (26 km, 14.3 Ma) is a large impact crater on Earth best suited for the study of processes of excavation (e.g., Hörz et al. 1983) and near-surface deformation of target rocks, as the amount of erosion is relatively small and access is ideal. The deposits of the continuous ejecta blanket, the so-called Bunte breccia, are widely preserved south and east of the crater but eroded in the north and northwest (e.g., Hüttner 1969; Gall et al. 1975; Pohl et al. 1977; Fig. 1). They extend up to 3 crater radii from the crater center. There are numerous sites where the underlying target rocks can be studied at known levels beneath contact with the ejecta blanket. Here, we report on deformation features of target rocks near the crater rim and in the periphery of the crater beneath the ejecta blanket (Bunte breccia) at distances ranging from 0.9 to 1.8 crater radii with respect to

the center of the crater. The results are compared with proximal ejecta layers of double-layer and multiple-layer ejecta craters on Mars.

The buried Chicxulub structure, Mexico, (180 km in diameter, 65 Ma old) has been identified as the impact crater related to the K/T boundary mass extinction and has been studied intensely by drilling and geophysical methods (e.g., Hildebrand et al. 1991; Pope et al. 1991; Kring 1995; Morgan et al. 1997). Surface exposures of its continuous ejecta blanket from the Albion Island quarry, northwestern Belize, were described first, and then were identified in adjacent Quintana Roo, Mexico, and in central Belize (Ocampo et al. 1996; Pope et al. 1999; Smit 1999; Schönian et al. 2003, 2004; Pope et al. 2005). Given a crater radius of approximately 90 km (Kring 1995), the ejecta blanket on the southeastern Yucatán Peninsula is exposed at distances R_{ej}/R of 3–5, which is in the upper range of typical values for maximum runouts of Martian fluidized ejecta blankets (ejecta mobility ratio $EM = R_{ej-max}/R$ of 1.5 to >6, respectively; Carr et al. 1977; Mouginiis-Mark 1987; Costard 1989; Barlow 2005). Therefore, the Chicxulub structure is the only known example on Earth where the distal portions of the ejecta blanket of a large impact crater are preserved, and it is thus regarded as ground truth for the processes of ejecta fluidization and the formation of ramparts on Mars (Pope and Ocampo 1999; Schönian et al. 2004).

RIES CRATER, GERMANY (26 km IN DIAMETER)

Geology of the Ries Crater

The Ries impact crater in southern Germany (Fig. 1) became one of the best-studied craters on Earth after Shoemaker and Chao (1961) proved its impact origin. It is a pristine, complex impact crater ~26 km in diameter that formed during the Miocene (14.34 ± 0.08 Ma; Laurenzi et al. 2003). According to Stöffler et al. (2002), the projectile was a binary asteroid that simultaneously formed the much smaller Steinheim crater (3.8 km in diameter) and a fan-like tektite strewn field (moldavites) in an oblique impact from WSW. The Ries impact occurred in a target with a two-layer configuration: a 620–750 m thick sequence of subhorizontally layered sediments (limestones, sandstones, and shales) of Triassic to Tertiary age, which most likely was fluid-bearing and which is underlain by crystalline basement rocks (gneisses, granites, and amphibolites; Pohl et al. 1977). Large parts of the Ries surface area were built up by Malmian (Upper Jurassic) limestones when the impact occurred.

The crater consists of an inner crater basin 12 km in diameter that is entirely formed in crystalline basement. The central basin, some 600–700 m deep, is outlined by a negative residual Bouguer gravity anomaly of -18 mgal (Kahle 1969), and a negative ground magnetic anomaly of -300 mgal (Angenheister and Pohl 1969). Recently, a structural uplift of 1.5–2 km of crystalline basement underlying the inner basin has been inferred from reinterpreted geophysical data and numerical simulations (Wünnemann et al. 2005). However, the lack of a morphologically visible central uplift is a striking feature of the crater that was not entirely understood until now. Deep drilling (Forschungsbohrung Nördlingen 1973) cored 600 m of the fractured crystalline basement and yielded a complete profile of the crater basin fill composed of 300 m of crater suevite and 300 m of post-impact sediments (Stöffler 1977). The inner crater basin is surrounded by an inner ring mainly built up by crystalline breccias. This crystalline ring forms isolated hills in the present landscape and is believed to roughly coincide with the maximum extent and overturned flap of the transient crater cavity (Wünnemann et al. 2005). A shallower annular trough, known as the “megablock zone,” is situated between the inner ring and the crater rim (Fig. 1). This megablock zone comprises both allochthonous blocks of brecciated crystalline and sedimentary rocks embedded in Bunte breccia deposits, as well as parautochthonous sedimentary blocks that have slumped into the crater during crater collapse. The hummocky relief of this area is an expression of its megablock nature. Concentric faults define the tectonic crater rim in several geoelectric traverses (Hüttner et al. 1980; Hüttner 1988) and a seismic section across the rim (Angenheister and Pohl 1969). The area outside the tectonic crater rim, the so-called Vorries zone, is covered by the continuous ejecta blanket (Bunte breccia),

allochthonous megablocks, and patches of suevite. The ejecta of the Ries crater is composed of clastic polymict breccias (Bunte breccia) that extend up to 3 crater radii from the impact center as an ejecta blanket of decreasing thickness. The partly noncoherent nature of the present exposure of the Bunte breccia resulted from erosion. Its thickness, which locally exceeds 100 m, scatters strongly and depends on the paleorelief (Gall et al. 1975). The constituents of the Bunte breccia are mainly unshocked to weakly shocked, upper-target sediments with minor amounts of crystalline rocks. The ratio of primary crater ejecta to local substrate components decreases with increasing radial range (Hörz et al. 1983). Local and crater-derived material are thoroughly mixed at all scales. The ejecta is interpreted as a “cold,” noncohesive impact formation (Hörz et al. 1983; Newsom et al. 1990). A clearly distinct type of ejecta represents the suevite, which predominantly consists of variously shocked and partly melted basement (von Engelhardt et al. 1995) and sedimentary material (Graup 1999; Osinski et al. 2004). Suevite achieves thicknesses of 300–400 m within the inner crater basin (crater suevite). Outside the crater, it occurs as patches that extend up to 2 crater radii (fallout suevite). The contact of suevite to Bunte breccia is sharp and indicates a hiatus and different ejection mechanisms between the emplacement of the Bunte breccia and the suevite. While the Bunte breccia deposits are considered to be formed by ballistic ejection which caused secondary cratering and an ensuing, turbulent debris surge (Pohl et al. 1977; Hörz et al. 1983) in a process known as ballistic sedimentation (Oberbeck 1975), the fallout suevite is believed to be settled as a turbulent suspension of melt lumps and solid particles in a medium of hot gases from an expanding vapor plume (e.g., Pohl et al. 1977; von Engelhardt 1990). In contrast, Osinski (2004) proposed that the fallout suevite was emplaced as ground-hugging impact melt flows.

Sharp contacts of the Bunte breccia ejecta blanket also occur with the underlying target rocks, even if the substrate is formed by unconsolidated sands (Hörz et al. 1983). Striations on contact surfaces reveal a radial flow. None of the contact planes of the limestone target to the Bunte breccia represents the ancient pre-impact land surface, since weathering horizons are lacking. The uppermost target layers were incorporated into the Bunte breccia ejecta flow. Wagner (1964) and Hüttner (1969) were among the first who observed subhorizontal shear planes also beneath the striated contact surface within Malmian target rocks.

Observation and Results

Subhorizontal and bedding-parallel shear planes (detachments) occur along the crater rim and in the periphery of the crater (Vorries zone) near the target surface beneath the continuous ejecta blanket. They exclusively formed in rocks with a rheological stratification caused by interbedded strata

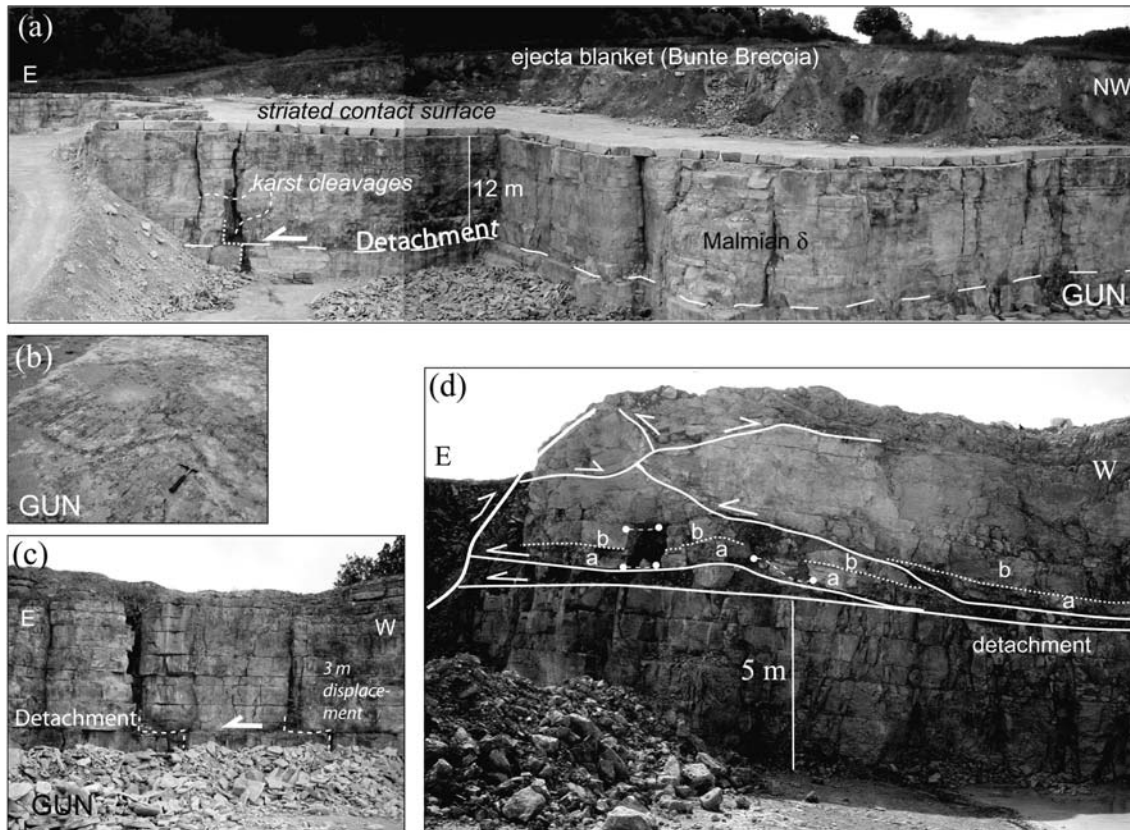


Fig. 2. a) An exposure of 8 m thick Bunte breccia above flat-lying Malmian δ limestones at Gundelsheim (GUN). The detachment occurs 12 m beneath the striated contact surface with visible offset in the E part. b) The contact surface (“Schlifffläche”) between Bunte breccia and target with striae striking 85° (GUN). c) A close-up of the major detachment at GUN at a different exposure. Note the offset of karst cleavages along the detachment horizon. d) Detachment and associated hanging wall deformation in Malmian δ limestone at Wemding (WEM). The detachment is truncated in E by a reverse fault that was active during crater collapse. Characters indicate strata that fit together and are used to restore the deformation. Minimum radial outward displacement is 4 m.

of thick limestone beds and thin marly interlayers. Shear zones are always localized along weak interlayers. Movements along the faults always show a radial slip vector with an outward displacement of the hanging wall block. This is indicated by 1) striations and grooves on shear planes (Fig. 2b), 2) offsets of major cleavage planes (Fig. 2a) and pre-impact karst caverns (Figs. 2a and 2c), and 3) the vergency of drag folding of the hanging wall strata. Detachments were also recognized by the occurrence of brecciated material injected along the shear planes (Fig. 2d). Detachments are formed some 1–70 m below the contact of the Malmian to the overlying Bunte breccia. Their depths beneath the ejecta blanket decrease with increasing distance from the crater center (Fig. 3a). The measured radial minimum displacement is in the range of 1–15 m (Fig. 3b). Note that some techniques merely allowed a calculation of the minimum displacement, and produce large error bars. The amount of displacement seems to decrease with increasing depth and distance from the crater center (Fig. 3). A decreasing displacement with depth suggests a genetic link between the emplacement of the ejecta blanket and the

occurrences of detachment planes. The interference of detachments with faults related to the collapse stage of cratering (Fig. 2d) indicates that detachment formation was the first deformation increment and started prior to the crater collapse but had not ceased when the crater collapse started (Kenkmann and Ivanov 2006). The structural observations suggest that detachment faulting of upper target layers is caused by weak spallation followed by outward dragging induced by the emplacement of the ejecta curtain.

A numerical analysis of near-surface target deformation around the Ries crater (Kenkmann and Ivanov 2005, 2006) provides further clues to the formation mechanisms and timing of detachment faults in the periphery of craters. Modeling has shown that movements of the uppermost target layers start with a material jump upward and outward a few seconds after impact (Kenkmann and Ivanov 2005, 2006). The horizontal motion decreases with depth, suggesting a mechanical decoupling of upper layers. This first deformation increment is caused by the interference of the expanding shock wave with rarefaction waves that are reflected from the target surface (which, per definition, is a zero pressure plane).

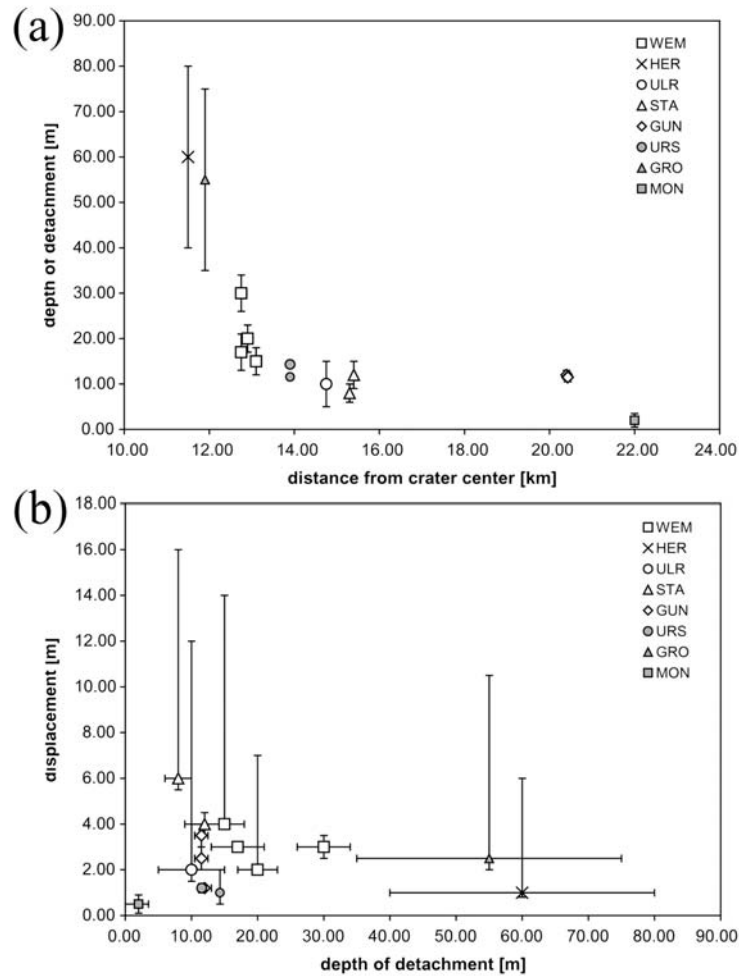


Fig. 3. A summary of structural data of analyzed detachment planes. a) Distance from crater center versus depth of detachment beneath contact to the Bunte breccia. b) Depth of detachment versus displacement along the detachments.

This process is known as spallation and leads to a mechanical decoupling of thin spall plates. Spallation is followed by a motionless period that lasts until the ejecta curtain passes the target tracer particles. The oblique trajectories of the impacting ejecta curtain material deliver a horizontal momentum to the uppermost target area and result in a second horizontal displacement increment by dragging. (Kenkmann and Ivanov 2005, 2006).

Implication for Mars

Thin-skin delamination and outward shearing of rocks beneath a continuous ejecta blanket is favored in targets with flat-lying sediments and rheological stratification in which the weakest layer controls the strength of a rock. Pore fluids reduce the effective stress to decouple thin surface layers. Thus, if detachment faulting operates in the periphery of Mars craters, it would most likely occur in layered sedimentary terrains saturated with volatiles.

Is it possible to detect subsurface detachments beneath ejecta blankets on Mars? Do they have a morphological expression which can be traced through an ejecta blanket? As the detachment is parallel to the surface, and is a relatively smooth plane covered by target and ejecta material, the detachment itself should be invisible in fresh craters. However, the associated deformation in the hanging wall layer and the overlying ejecta, which is particularly concentrated in the front and rear of a detachment and along obstacles, undulations, and ramps, may have a morphological expression. The critical length of a detachment, which gives the spacing of enhanced deformation, can roughly be estimated by the strength properties of the block in motion. Pushing a block of unit width, length l , and thickness z along a plane, resisted by a basal friction coefficient μ , a critical length of the block can be determined assuming the simple effective stress law (Scholz 1990):

$$l_{crit.} = (\sigma_{hor} \times z) / ((\sigma_{vert} - p) \times \mu) \tag{1}$$

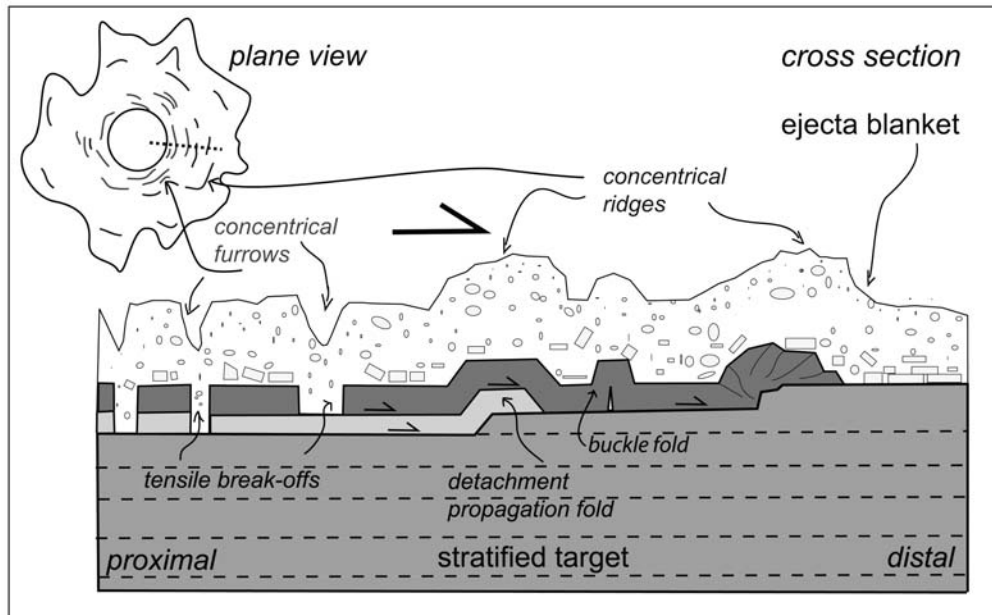


Fig. 4. A sketch illustrating the formation of concentric ridges and furrows by detachment faulting beneath an ejecta blanket in a radial cross section. The formation of detachments and associated radial outward motion is caused by spallation and subsequent ejecta dragging of near-surface block. Rock accumulation above ramps and in front of a detachment leads to folding. Tensile break-offs may produce graben-like furrows in the rear of detachments.

where σ_{hor} and σ_{vert} are the horizontal and vertical stresses and p is the pore fluid pressure. σ_{vert} corresponds to the lithostatic load and correlates to the depth of the detachments. The length of the hanging wall block is limited by σ_{hor} which must not exceed the strength of the rock, or basal shearing ceases and internal fracturing occurs. Independent of crater size we estimated a critical block length of $\sim 3000 \text{ m} \pm 300 \text{ m}$ for detachment depths of 10–70 m, respectively, applying experimental strength data for limestone (Handin et al. 1963). The length increases in the presence of a fluid phase that may lubricate the detachment and reduce the effective stress. The crude estimate of detachment length neglects the influence of a diverging flow, buckling instabilities, and the assumption of pushing forces is oversimplified. In any case, if failure of thin layers during outward motion occurs, faults propagate from the detachment to the target surface and cause yielding of rock material. This material is pushed upward to the free surface to form a morphological ridge of more or less concentric strike (Fig. 4). Alternatively, fault-propagation folds may evolve at the tip of such detachments or along ramps in the detachment plane (Fig. 4). Moreover, buckling instabilities may arise in the thin detached layer depending on layer thickness and rheological competence contrasts, leading to buckle folding (Fig. 4). Various types of folds can develop that are likely to produce morphological ridges with strike axes perpendicular to the dominant transport direction. In contrast, in the rear of a detachment at a more proximal distance to the crater, outward motion on detachments should lead to cut-offs of the hanging wall which may lead to concentric troughs or furrows at the surface around the crater.

Are there any indications for this hypothetical type of deformation beneath ejecta blankets? Figure 5 displays Mars Orbiter Camera (MOC) (Malin et al. 2001; Fig. 5a) and Thermal Emission Imaging System (THEMIS) images (Christensen et al. 2004; Fig. 5c) of the 25 km diameter Tartarus crater in the northern lowlands (37.4°N , 159.1°E). The crater's low average elevation of -3000 m makes it a likely host of volatiles and a target composed of sedimentary layers. The close-up of the inner ejecta layer displays straight radial grooves (Fig. 5c) and ridges that are interpreted as the product of erosion by supersonic surge on the inner layer (Boyce and Mouginis-Mark 2005). Radial grooves of the inner layer are interrupted at furrows and ridges which have a concentric to lobe-parallel strike. Lobe-parallel furrows and ridges indicate that the ejecta was probably sheared radially outward and is stripped off the target (Fig. 5). Furrows dominate in the more proximal part whereas ridges are concentrated in more distal areas. The width of the major furrows is on the order of 300 m and roughly corresponds to the spacing of Mars Orbiter Laser Altimeter (MOLA) data points (Fig. 5b). The depth of the transected furrows is 20–40 m in the MOLA profiles. However, taking into account that each MOLA data point represents the average of a 150-meter-wide bin, the true depth of furrows might be remarkably deeper. Hence, some furrows may cross-cut the entire ejecta blanket. Whether the furrows propagate into the target is a matter of debate because the elevation of the target surface is unknown. Lobe-parallel ridges have a height of about 10–30 m. The radial distance between furrows and ridges is about a few kilometers. The width of a furrow

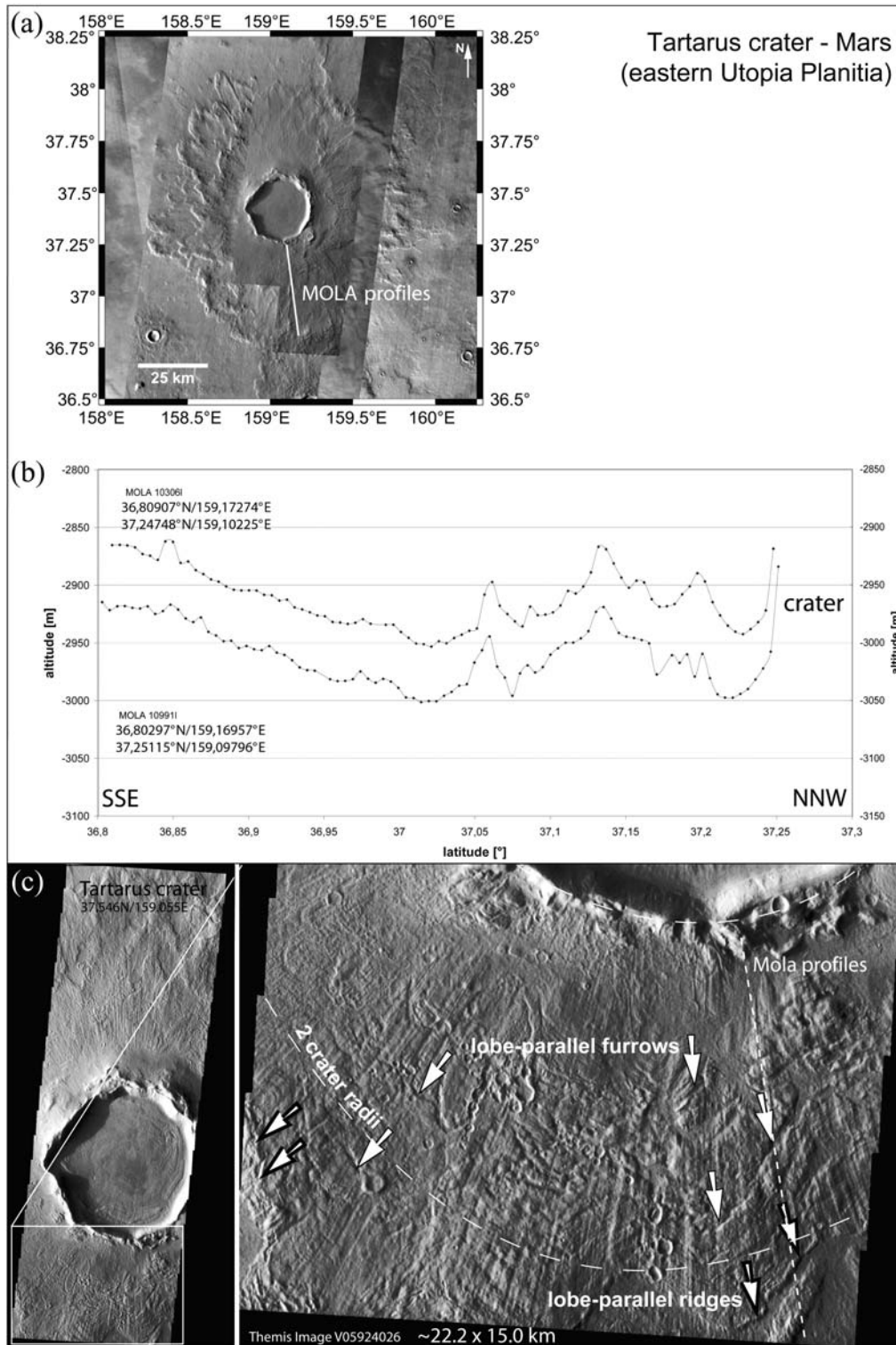


Fig. 5. a) A context image of the 25 km Tartarus crater (north of the Elysium region), composed of MOC-wide angle (MOC-WA), THEMIS-IR daytime, and THEMIS-VIS images. b) Two nearly parallel MOLA tracks provide NNW/SSE profiles across the inner ejecta layer. The spacing of MOLA data points is ~ 300 m. c) A close-up view of the inner ejecta facies south of the crater. The ejecta displays an uneven surface with radial striations and grooves that are interrupted by lobe-parallel furrows and ridges. Image credit: MOC-WA: M0906229, R1403041, R1901505, Malin et al. 2001 (NASA/JPL/MSSS). THEMIS-IR: I11603006, I10380008; I11940012; I09731013; THEMIS-VIS: V05924026, V12514003, Christensen et al. 2004 (NASA/JPL/ASU).

defines the magnitude of outward shearing of the more distal part (southern furrow wall) with respect to the more proximal part of the ejecta. Hence, outward shearing at the target-ejecta interface or beneath the ejecta is about 300 m at a single furrow. This is a much higher displacement magnitude than the minimum decoupling distances derived for the Ries crater. Possible reasons for this discrepancy could be a higher volatile content of the Martian target or differences in the ejecta flow dynamics. The latter is particularly suggested by the presence of radial grooves imprinted on the surface of the inner ejecta lobe, which testifies to an additional dragging effect of the outer ejecta on the previously deposited inner ejecta. To summarize, we propose that lobe-parallel furrows and ridges may have formed by radial sliding at the target-ejecta blanket interface and along near-surface target detachment beneath the ejecta blanket.

If the Ries crater is an analogue to double-layer (or multiple-layer) ejecta craters on Mars, this should be indicated by the presence of two ejecta layers. The abrupt change from strictly radial to a deflected flow, which can be inferred from the Tartarus crater (Fig. 5) and other craters (e.g., the Bacolor crater; Boyce and Mougins-Mark 2005), cannot be reproduced in the Ries crater. In contrast, deflections of striations and grooves by up to 30° from a pure radial direction were measured irrespective of radial distance around obstacles of the preexisting paleorelief (Wagner 1964; Hüttner 1969). Extensive NASA drilling yielded complete vertical profiles through the Bunte breccia (Hörz et al. 1983), but no boundaries between different ejecta layers, such as glide planes or horizons with laminar flows, were recorded. As introduced before and detailed, e.g., by Hörz (1982), an ejecta layer of suevites rests in sharp contact with the Bunte breccia ejecta layer. The fallout suevite is volumetrically of subordinate importance and most likely has formed a primarily patchy, discontinuous layer. Bunte breccia and suevite definitely represent two phases of ejecta with different ejecta composition and emplacement process. However, aerodynamic sorting of the suevite ejecta and surging upon landing on the Bunte breccia can be neglected since the suevite shows extremely poor grain-size sorting (Hörz et al. 1983), contains delicate aerodynamically formed bombs, and shows no mixing with the underlying Bunte breccia. Hence, although a twofold ejecta occurs both at Ries and on Mars, mechanisms of formation may be different.

EJECTA BLANKET OF THE CHICXULUB CRATER, MEXICO (180 km IN DIAMETER)

Geology of SE Quintana Roo and the Chicxulub Ejecta Blanket

The Chicxulub ejecta blanket in the Rio Hondo region (SE Quintana Roo, Mexico) is exposed in an area that hitherto was mapped as Neogene (López Ramos 1975; INEGI 1987; cf. Pope et al. 2005; Fig. 6). This apparent paradox was

previously attributed to tectonically uplifted blocks, bounded by large-scale reverse faults (Ocampo et al. 1996; Pope et al. 2005). However, since most of the carbonates of the southern Yucatán Peninsula are heavily weathered and/or recrystallized, well-preserved fossils are rare and only the age of the Neogene Bacalar Formation west of the Bacalar Lagune and along the Rio Hondo is well constrained (Alvarez 1957; Butterlin 1958; Fig. 6). Limestones, dolomites, marls, and evaporites exposed across the southern Yucatán Peninsula lack reliable biostratigraphic data but might in part be correlated with Upper Cretaceous rocks in the subsurface of the northern peninsula (López Ramos 1975; Schönián et al. 2005).

Upper Cretaceous rocks beneath the ejecta blanket are karstified. This was recognized by fractures and solution breccias and the presence of a caliche layer immediately below the ejecta blanket at Albion Island in Belize (Pope et al. 1999; Fouke et al. 2002). A pre-K/T subaerial exposure of this part of the Yucatán Peninsula is even more clearly expressed by a pronounced paleorelief and karst features as caliche layers, travertine deposits, dissolution vugs, and even dolines below the ejecta blanket at various localities in Quintana Roo (Pope et al. 2005; Schönián et al. 2003, 2005; cf. Esteban and Klappa 1983; Mylroie and Carew 1995). The Chicxulub ejecta in part surrounds hills of karstified limestones that overlie the dolomitic Barton Creek Formation and erroneously have been dated as Paleocene based on planktonic foraminifer tests (Agua Dulce locality, Fig. 6; Smit 1999, personal communication; Schönián et al. 2005; cf. Pope et al. 2005). The observation that the heavily karstified rocks are overlain and/or surrounded by the K/T-age Chicxulub ejecta blanket, the absence of overlying Paleogene rocks, and a morphological mapping approach using remote sensing data resulted in a revised geological model for southeastern Quintana Roo (Schönián et al. 2005; Fig. 6). Following this scenario, the platform carbonates were uplifted and subaerially exposed along major reverse faults (the Kohunlich and Rio Hondo faults) during two events in the Upper Cretaceous.

Until recently, unequivocal evidence for an impact origin of the Chicxulub ejecta was only provided for the Albion Island and Armenia localities in Belize by the presence of quartz grains with shock metamorphic effects (planar deformation features [PDF]; Pope et al. 1999; 2005). Systematic search for shock indicators also yielded quartz with PDF for various localities of the ejecta blanket in Quintana Roo, Mexico (Figs. 6 and 7). Additionally, highly shocked crystalline basement clasts and altered melt particles were found at three ejecta localities in the Rio Hondo region (Sarabia, Ramonal, Agua Dulce; Fig. 6). These findings of crater-derived debris confirm the impact origin of the localities identified by either petrographic (Pope et al. 1999, 2005) or sedimentologic criteria (Schönián et al. 2003, 2005), and currently provide the only reliable stratigraphic marker for this region. The poor outcrop conditions of the ejecta

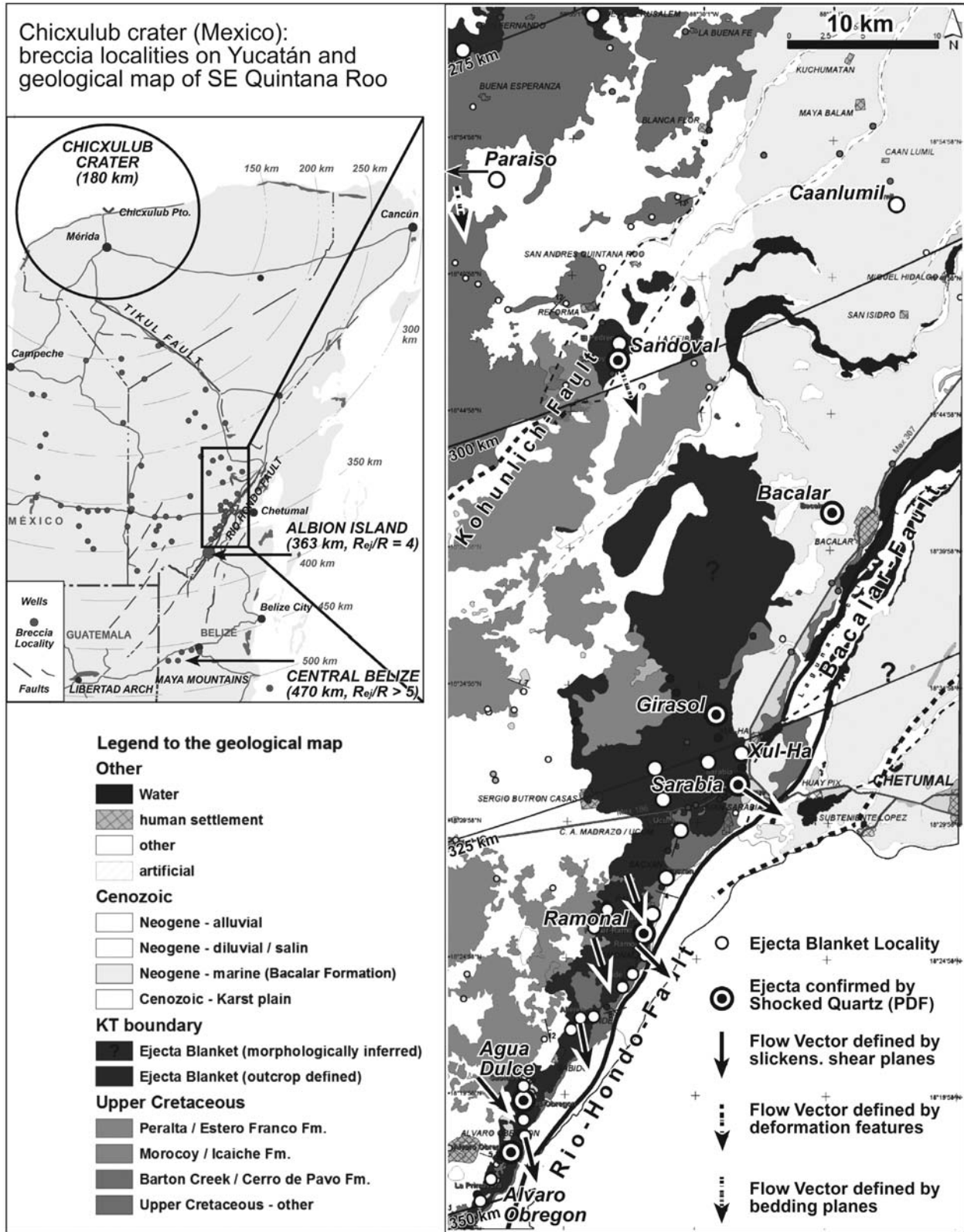


Fig. 6. A map of the Yucatán Peninsula with the location of the Chicxulub impact crater, study area, and confirmed ejecta blanket localities in Belize (Pope et al. 2005). The geological map of southeastern Quintana Roo was derived from field mapping in combination with remote sensing data (Landsat ETM+ satellite images and SRTM-DEM). Only in the east and northeast Neogene strata (Bacalar Formation) cover the ejecta blanket. Ejecta localities, including those with findings of shocked quartzes and reconstructed flow vectors, are highlighted.

blanket and its continued karstification, weathering, and erosion inhibit measurement of its maximum thickness and thus prevent estimates of the ejecta volume and study of its surface properties. This hampers direct comparison with morphologic information from remote-sensing, morphometric data (MOLA), and thermophysical properties (THEMIS) of Martian ejecta blankets (e.g., Garvin et al. 2000; Barlow 2005; cf. Fig. 5). However, the unequivocal identification of the Chicxulub ejecta blanket and its aerial mapping in southeastern Quintana Roo does for the first time allow study of the lateral and proximal-distal variability of its petrographic and sedimentary properties.

Observations and Results

The Chicxulub ejecta blanket in the study area is a very heterogeneous, oligomict-to-polymict diamictite or breccia with a high variability in particle roundness and shape, matrix composition, and internal structures, and contains dolomite boulders of up to 12 m in size. Grain size distributions of the diamictite measured in the well-exposed Albion Island quarry exhibit two clast populations and reveal the heterogeneous, completely unsorted, and chaotic nature of the ejecta blanket (Pope et al. 1999; King et al. 2003). A twofold stratigraphy of the Chicxulub ejecta blanket has been proposed based on a basal layer 0.1–1.7 m in thickness below the bulk ejecta material in the Albion Island quarry that contains abundant dolomite spheroids which, in analogy to volcanic plumes, have been interpreted as carbonate “accretionary lapilli” of a primary vapor cloud (Pope et al. 1999, 2005). In Quintana Roo such spheroids have been found within a clay-rich basal portion of the ejecta blanket at three localities (Girasol, Xul-Ha, Ramonal; Fig. 6). These deposits comprise local pockets rather than a laterally continuous layer. Thus, the spheroid-bearing units are either erosional remnants that were deposited within paleokarst depressions or might be of a different origin (cf. Fouke et al. 2002; Schönian et al. 2004).

While silt-sized quartz grains with PDF have been found throughout the study area (Sandoval, Girasol, Sarabia, Ramonal, Agua Dulce, Alvaro Obregon, Bacalar; Figs. 6 and 7), larger crater-derived debris is sparse and was found only beyond 3.5 crater radii from the impact center. Clay particles that occur within the spheroid-rich bed and are dispersed throughout the diamictite matrix were interpreted as altered glass shards (Ocampo et al. 1996). They are mostly smectites (rarely palagonite) and sometimes display vesicles and spherulitic devitrification structures (cf. Pope et al. 1999). However, smectites derived from limestone dissolution are present within the karstified subsurface, became incorporated the basal ejecta blanket, and are difficult to distinguish from altered melt particles based on XRD and XRF analyses (Schönian et al. 2004, unpublished data; cf. Isphording 1984). Therefore, the actual amount of impact melt within the distal Chicxulub ejecta blanket cannot yet be determined to a satisfactory degree.

Much of the ejecta blanket material is eroded from the local bedrock and associated karst lithologies (Schönian et al. 2003, 2005). Karst features such as travertine, speleothemes, carbonate nodules, and black limestones do occur as clasts within the ejecta blanket. Unconsolidated white chalk and residual clays which can be found as dolina infills in the Upper Cretaceous rocks become successively incorporated within the ejecta blanket with radial distance (Schönian et al. 2003, 2004; cf. Esteban and Klappa 1983). To draw conclusions about the processes that acted during ejecta emplacement, this study focuses on internal structures and sedimentary characteristics of the ejecta blanket.

At 3.0–3.3 crater radii from the impact center (280–300 km, northern study area), the ejecta blanket lacks crater-derived debris, is clast-rich, and is less consolidated than in the south. On an uplifted plateau in the northwestern study area (Fig. 6; Paraiso locality outside the map), a succession of alternating marls, clays, and limestones occurs that displays soft sediment deformation features such as boudinage, folds, and synsedimentary faults. This succession indicates mass movement from NNW to SSE and is overlain by a breccia that is composed of lithologies of the underlying rocks. East of the plateau, the ejecta blanket fills a smoothly karstified plain. In the northeast, a clast rich breccia with 2–3% of clay particles is overlain by white, fossiliferous marls of the Bacalar Formation that occasionally contain resedimented ejecta blanket material (Caanlumil and Bacalar localities; Fig. 6).

At a distance of 3.3 crater radii (298 km) from Chicxulub, a similar oligomict breccia that contains ~2% altered glass fragments and rarely quartz with shock metamorphic features is exposed in a large quarry and several smaller outcrops (Sandoval locality; Figs. 6, 7a, and 8a). No striated shear planes are present, but irregular, large-scale bedding structures defined by lithological changes in matrix composition and clast content can be observed. The dolomite and limestone clasts are subangular to angular and only rarely display faint abrasion features. Only a few clasts larger than 50 cm and no matrix-coated or clay-coated boulders were found.

At a distance of 3.5–3.6 crater radii from the impact center (315–325 km, Chetumal area, Sarabia quarries), the ejecta blanket covers morphologically elevated dolomites of the Barton Creek Formation (Fig. 6). It comprises a white, well-consolidated, and completely unsorted chalky diamictite which contains mottled dolomite boulders of up to 3 m in diameter that sometimes display matrix coatings. Weathered granitoid and altered melt clasts do occur for the first time at these distances within the ejecta blanket. Approximately 5% clay particles are dispersed within the matrix that, in part, represent altered impact glasses. At an exposed basal contact with the underlying brecciated and karstified Barton Creek dolomites near the Sarabia quarries, deeply grooved shear planes and pockets of locally derived clay breccias can be observed (Schönian et al. 2004; Fig. 10c). The well-exposed Barton Creek Formation displays evidence of subaerial

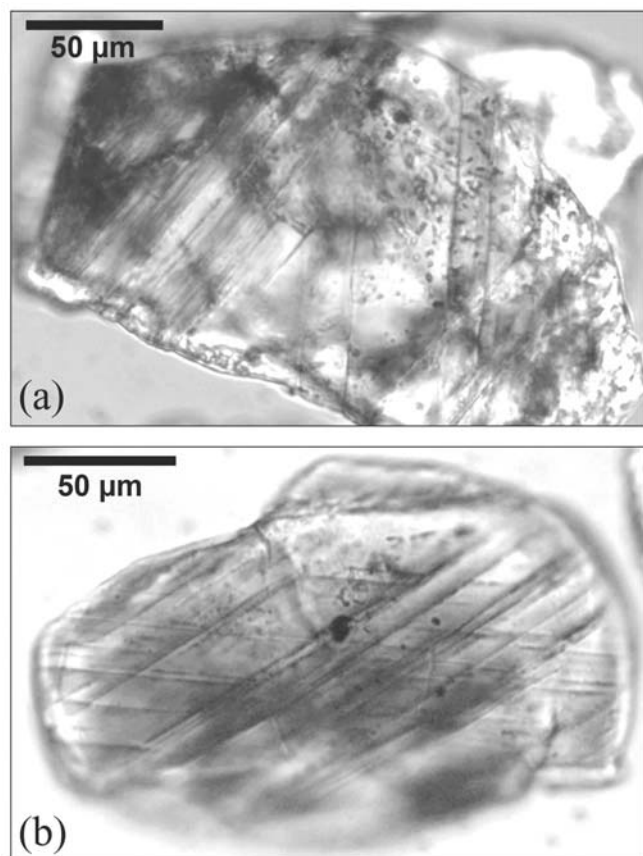


Fig. 7. Examples of quartz grains that exhibit planar fractures (PF) and planar deformation features (decorated PDF). The shocked quartzes were selected from the <math><150\ \mu\text{m}</math> fraction of insoluble residues of the ejecta matrix and are mounted in oil (obliquely crossed polarized light). a) Sandoval locality at 3.3 crater radii from Chicxulub (298 km). b) Girasol locality at 3.5 crater radii from the impact center (322 km; see Fig. 6).

exposure in its upper part, such as dolomitic limestone beds with mottled textures, caliche interbeds, iron oxide staining, and dolinas and karst conduits with chalk or clay fillings (cf. Esteban and Klappa 1983; Mylroie and Carew 1995).

Farther south of the crater, at 3.6–3.9 radii (330–350 km) from Chicxulub Puerto, the Upper Cretaceous paleorelief becomes more pronounced and exhibits hills elevated above the ejecta blanket and paleovalleys filled with ejecta blanket material. The matrix composition is usually chalky dolomitic, but displays a high variability and locally tends to include more marly and clayey material. Linear, curved, and, in part, highly chaotic shear planes often connected with polished and striated surfaces, sheared ejecta material, and clay-rich shear breccias become a major sedimentological feature (Fig. 8b). Large dolomite boulders are abundant, some with matrix or clay coatings. At the Ramonal road cut a spheroid-rich basal ejecta unit fills a depression and, towards the south, covers a hill of recrystallized dolomitic limestones that displays a pronounced paleorelief and abundant karst features (Figs. 6

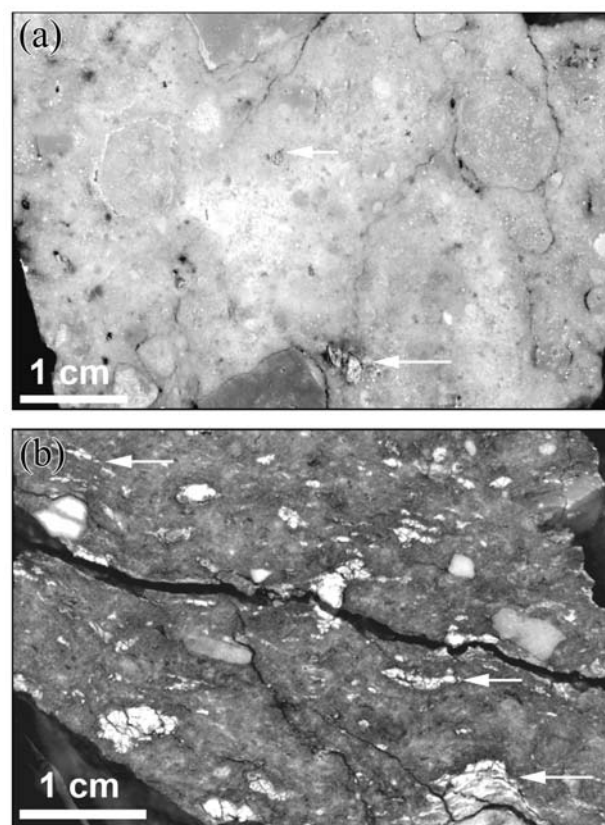


Fig. 8. Polished slabs of two examples of the matrix of the ejecta blanket. a) A oligomict, fairly well-consolidated, unsheared diamictite from the Sandoval quarry (Fig. 6) with rare altered glass shards (arrows). b) Sample of the red oxidized, clay-rich basal gliding plane beneath the lower, spheroid-rich ejecta layer at the Ramonal road cut (W wall; see Fig. 9). Note that while some clay clasts are rather intact, other clay particles are flattened and show a shape-preferred orientation which indicates internal shear stress.

and 9a). The “spheroid bed” atop this obstacle shows intense internal shearing and is bound by thin sheared layers composed of locally eroded clays and paleosoils (Figs. 8b and 9b). At distances >3.5 crater radii from the impact center, internal shear planes become a predominant feature within the ejecta blanket. The amount of clay particles within the diamictite matrix rises to 10–20%, but clays are inhomogeneously distributed and often concentrated in pockets, layers, or along gliding planes that reflect the heterogeneous nature of the eroded karstified bedrock. At Agua Dulce, a major subhorizontal glide plane that extends over more than 90 m and numerous associated secondary shear planes is present (Figs. 6, 10a, and 10c). Within well-consolidated, carbonate-rich, and clay-poor portions of the ejecta blanket, discrete localized shear planes with thin clay partings and/or deeply grooved shear surfaces are developed, whereas ejecta matrices with clay content larger than ~15% display bedding planes, chaotic slumps, and structures related to turbulent flow (Schönian et al. 2003, 2004).

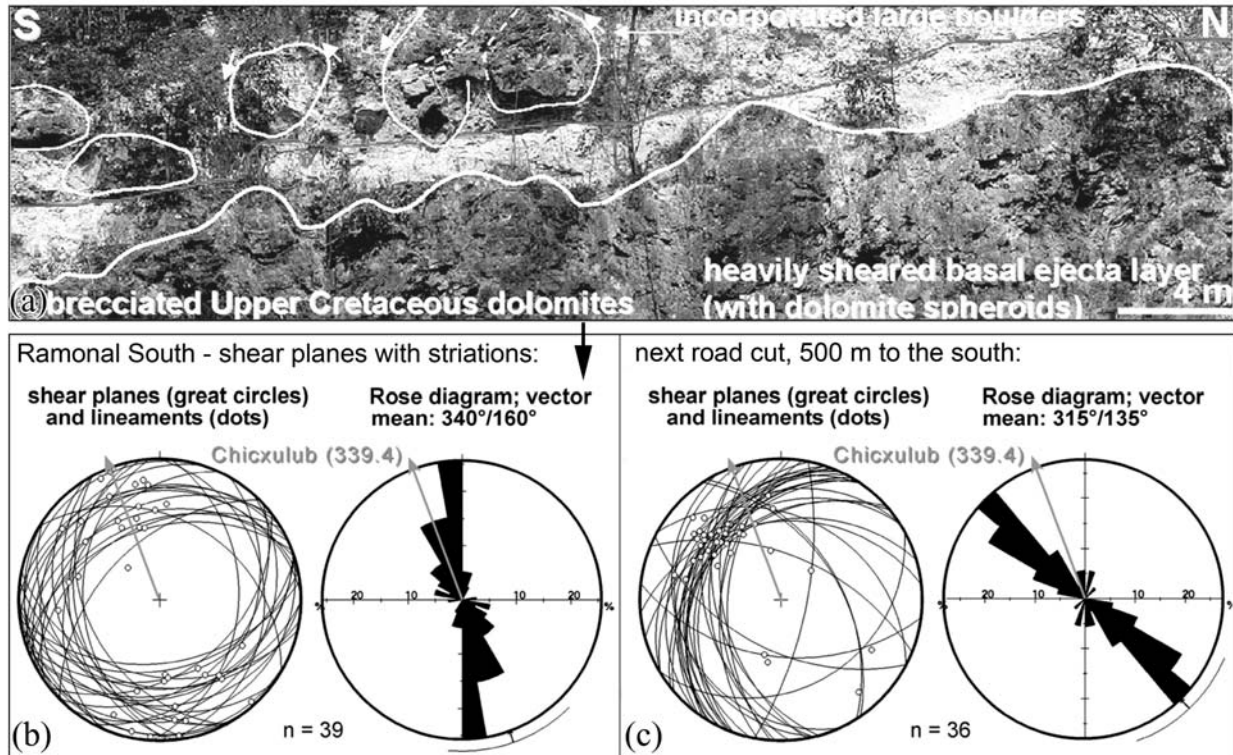


Fig. 9. a) A panorama of the western wall of the Ramonal road cut (335 km, 3.7 crater radii from Chicxulub). The ejecta blanket covers a relief of karstified dolomitic limestones. The lower, spheroid-bearing layer is strongly sheared. It is bounded by a subhorizontal gliding plane that is composed of sheared clay breccias (Fig. 8b). Atop this layer, large, eroded dolomite boulders slide within a very chaotic diamictite. b) Clearly developed slickensides on the surface of discrete shear planes have been measured within the basal, spheroid-rich bed. Data are displayed as plane/line plots and Rose diagrams. c) Data taken from the next outcrop, just 500 m south, show a significant deviation from the Ramonal locality and from the radial-outward movement from the impact center (see Fig. 6).

Particle Abrasion

Clasts with abrasion features such as polished and faceted surfaces, striations, pits, and grooves first occur at 3.5 crater radii from the impact center in the Sarabia quarries near Chetumal and become frequent towards the S (Figs. 6 and 10b). Abraded clasts are usually associated with well-developed shear planes and may show chaotically curved, deep grooves. Some well-rounded pebbles with polished and striated clast surfaces were extracted from straight shear planes. This has been regarded as evidence that particle abrasion is related to the nature of the secondary ejecta flow and not to processes that occur during ballistic transport of crater-derived material (Schönian et al. 2003). Systematic measurement of roundness and sphericity of dolomitic pebbles from various localities reveals that the amount of abraded clasts rise with crater distance. However, angular and subangular clasts are also frequent at distant localities, which indicates the presence of debris that was eroded from the nearby brecciated subsurface and not transported over large distances. Strongly abraded clasts are reported from the upper impactoclastic layer at localities in central Belize that yielded abundant quartz grains with shock metamorphic features (Pope and Ocampo 2000; Pope et al. 2005).

Ejecta Flow

To infer flow trajectories, internal structures such as subsurface deformation features, bedding planes, and slickensided or grooved shear planes were measured systematically. As a result, the data obtained from subsurface deformation and bedding structures in the northern study area still seem to indicate a radial flow away from the impact center. The slickensided shear planes that preferentially occur at the base of the ejecta in the Chetumal area and the Rio Hondo region in turn display remarkable deviations around obstacles like paleokarst hills (e.g., 38° for Sarabia, 24° for Ramonal S, or 19° for Agua Dulce; Figs. 6b and 9b).

In summary, detailed geological mapping of SE Quintana Roo revealed that the Chicxulub ejecta overrode, eroded, and in part nivalled a karstified Upper Cretaceous land surface that became sealed off as “covered karst” and only in the northeastern study area was again transgressed by a Neogene sea (Schönian et al. 2005; Fig. 6). The observations on internal structures and abrasion features of the Chicxulub ejecta blanket indicate that the secondary ejecta flow was noncohesive and turbulent up to approximately 3.4 crater radii from the impact center (a distance of 310 km). Probably by detrainment of volatiles or a primary reduced volatile

content of the more distal ejecta, it then evolved to a cohesive debris flow (Fig. 11b). Particle abrasion rising with crater distance can be related to internal friction and the abundance of locally eroded clays that lubricate shear planes and cause strain partitioning within the flow. Shear planes dominantly occur near the base of the ejecta (Figs. 9, 11a, and 11b). This points towards the important role of locally derived material for the emplacement of the Chicxulub ejecta blanket and its large runout efficiency. Localization of the flow along large-scale discrete glide planes indicates that perturbation by secondary impacts is impeded at this distance (Figs. 9a, 10a, and 11a).

Implication for Mars

The analysis of the Albion island outcrop (Ocampo et al. 1996, 1997; Pope et al. 1999; Pope and Ocampo, 2000; Pope et al. 2005) led to the conclusion that the distal portion of the Chicxulub ejecta blanket was deposited by a primary impact vapor cloud and a subsequent turbulent debris flow that resulted from ejecta curtain collapse. This interpretation is based on the twofold stratigraphy and the apparent absence of subsurface erosion at the Albion Island outcrop, on the interpretation of dolomite spheroids as “accretionary lapilli” and of matrix-coated or mud-coated boulders as “accretionary blocks”, and the assumption that abrasion features on dolomite clasts are caused by particle interaction within the ejecta curtain. Consequently, the ring vortex model emphasizing the role of atmospheric turbulence in the formation of Martian ejecta blankets was regarded as being valuable for Earth as well (Pope and Ocampo 1999; cf. Schultz and Gault 1979; Schultz 1992; Barnouin-Jha and Schultz 1996, 1998). In contrast, our observations from Quintana Roo, Mexico, suggest that at these distances, the Chicxulub ejecta blanket was deposited by a secondary, ground-hugging, cohesive, and erosive debris flow that followed ballistic emplacement. No proximal-distal grain size grading with finer material in the outer ejecta facies as would be expected for a turbulent, atmospheric debris flow (Barnouin-Jha and Schultz 1996, 1998; Barlow 2005) can be found within the Chicxulub ejecta. Contrary to the ring vortex model, large boulders seem to be rare up to 3.5 crater radii from crater center but become eroded from the subsurface towards the south, and are probably responsible for the two clast populations observed at Albion Island (Schönian et al. 2003; King et al. 2003; cf. Pope et al. 1999). Barlow (2005) stresses that low thermal inertia of Martian ejecta blankets derived from THEMIS measurements do not allow one to easily distinguish between primarily fine-grained distal ejecta as predicted by the ring vortex model and dust-covered ejecta blankets. However, high thermal inertia and rough surfaces of either fresh or degraded distal ejecta blankets on Mars might be indicative of coarse material eroded by the secondary ejecta flow.

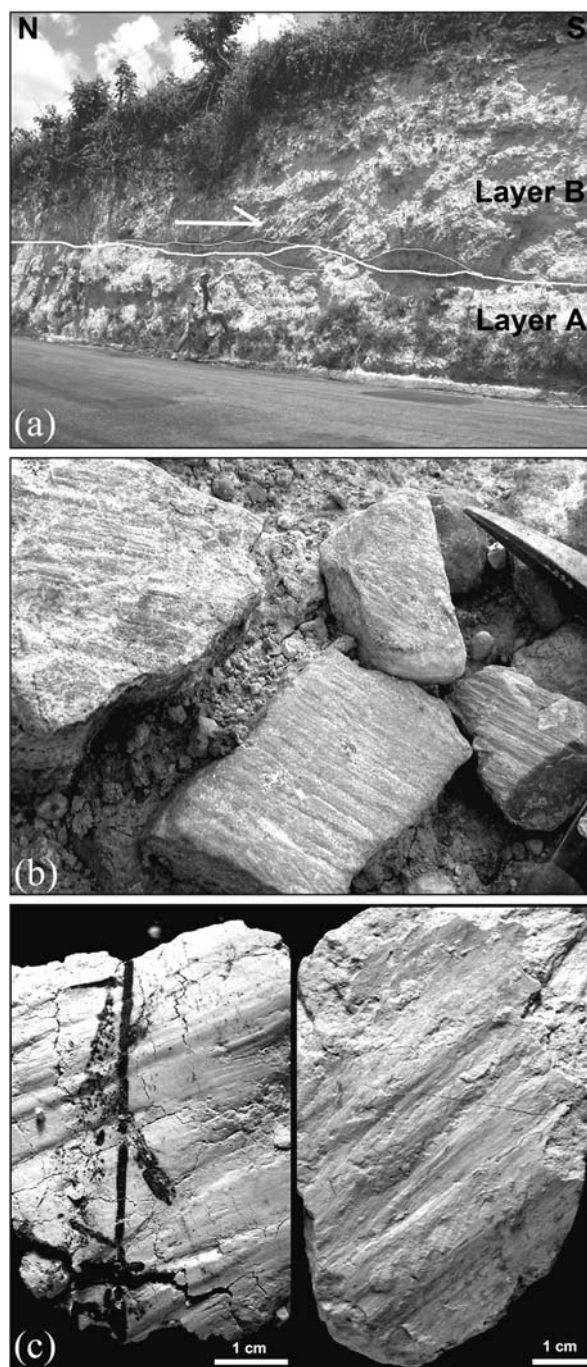


Fig. 10. a) An outcrop view of the northern end of the Agua Dulce road cut (343 km, 3.8 crater radii from the impact center) exhibiting a subhorizontal gliding plane that separates a coherent, clay-poor lower layer which contains numerous, discrete shear planes (Layer A), and a chaotic, clay-rich upper portion (Layer B). The main gliding plane (thick line) displays anastomosing embayments leading to isolated lensoid bodies bounded by secondary shear planes (thin lines). b) Faceted and striated dolomite and limestone clasts from the Sarabia quarry (328 km; 3.65 crater radii from Chicxulub). Some of the clasts display striations in more than one direction. c) Examples of slickensided and grooved shear planes within the ejecta matrix from Agua Dulce (left) and Sarabia (right).

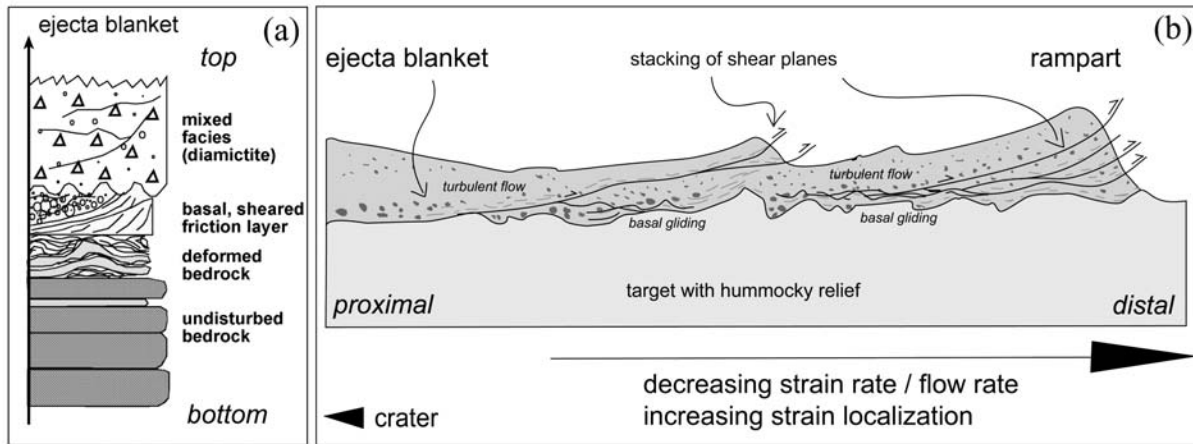


Fig. 11. a) Schematic profile through the Chicxulub ejecta blanket synthesized from various outcrops. b) Hypothetical radial cross-section through a fluidized ejecta blanket displaying the proximal-to-distal and top-to-bottom transition from a turbulent flow to a localized flow as inferred from the Chicxulub ejecta blanket. Ramparts may form by a stacking of shear planes. Compare the expected topography with the distal portion of the MOLA profiles across the ejecta blanket of the Tartarus crater on Mars (Fig. 5b).

The significant deviation of the Chicxulub ejecta around paleokarst hills (Figs. 6 and 9) indicate that, at these distances from the impact center, the secondary flow was already slow enough to be affected by topography. This is consistent with the observation that on Mars the outer portions of the fluidized ejecta blankets are deflected by obstacles and become channelized (Carr et al. 1977; Wohletz and Sheridan 1983; Mouginiis-Mark 1987), which was seen as evidence for a high-density, low-velocity surface flow. At the Tartarus crater (Fig. 5), the pronounced radial texture of the inner ejecta facies is in contrast to a thinner outer ejecta layer, on which flow lines are deflected around topographic highs. These two distinct ejecta morphologies were also observed at double-layer ejecta craters like Bacolor (33.0°N, 118.6°E). Here, channelized outer ejecta that is attributed to subsonic flow displays deviations around obstacles of up to 30° (Boyce and Mouginiis-Mark 2005).

The results presented from Chicxulub favor the role of subsurface volatiles and eroded bedrock lithologies for the development of the secondary ejecta flow. Unequivocal evidence that atmospheric turbulences contributed to the final emplacement of the preserved portions of the distal ejecta blanket has not yet been found. The study of the Chicxulub ejecta blanket, therefore, does not support the perception that atmospheric processes are responsible for the formation of fluidized ejecta blankets. The circumstance that atmospheric density and pressure on Mars was much lower than on Earth throughout most of its geologic history (Jakosky and Phillips 2001) further stresses the unlikelihood of atmospheric processes as the main agent for the fluidization of Martian ejecta blankets.

Mechanical Implications

The presence of layered ejecta on Mars with different degrees of fluidization is often correlated with the water/ice

content of target rocks as a function of depth. The less-fluidized state of the inner ejecta indicates that it contains less water than the outer ejecta blanket. The inner ejecta layer is fed by weakly shocked-to-unshocked, low-velocity ejecta from the rim zone of the transient crater cavity which, thus, contains less shock-melted ice (Stewart et al. 2001). In contrast, the highly fluidized outer ejecta layers should contain more water because they are fed by an ice-rich target that is probably completely shock-melted.

On Earth, under standard climatic conditions, shock melting of ice is irrelevant to provide water as a fluidization agent of ejecta blankets because water is already present. But the primary volatile content decreases with depth due to the successive closure of fractures and pore space. Hence, the inner portions of terrestrial ejecta layers should contain more water, and thus should be more fluidized than the outer regions. As outlined above, this could, in fact, be inferred from the Chicxulub ejecta blanket.

The mechanical properties of fluidized ejecta blankets on Mars were described as a Bingham rheology (Ivanov et al. 1994) with parameters for cohesion and kinematic viscosity similar to terrestrial lahars and water-saturated debris flows (Ivanov and Pogoretsky 1996; Ivanov et al. 1997). Contrary to Newtonian fluids, Bingham fluids are characterized by a yield stress. In order for Bingham fluid to flow, the driving shear stress has to be larger than this yield stress. Below the yield, the fluid behaves almost like a solid body; above the yield, the fluid behaves as a linear viscous flow. Is this rheological description compatible with the observed structural features of the Chicxulub ejecta blanket? The chaotic fabric in large parts of the ejecta indicates a liquid-like flow above the Bingham yield. The occurrence of glide planes near the base of the ejecta flow, however, suggests a different flow regime (Fig. 11). Basal gliding and strain localization could be interpreted as deformation near the critical yield stress.

Likewise, the frequent occurrence of glide planes with increasing radial range suggests that the physical boundary conditions have changed towards the distal portions of the flow (Fig. 11b). We propose that a transition from a turbulent, chaotic flow to a friction-controlled, localized flow along internal shear planes and shear plane networks is mainly controlled by a decreasing flow rate within the ejecta. A reduced shear strain rate can be inferred from the topography-controlled flow and the observed >90 m-long glide plane because the length of a shear zone inversely depends on shear strain rate (Fig. 10a; Melosh 2005). The formation of morphological ramparts could then be due to an imbrication and stacking of ejecta layers bounded by glide planes or glide plane networks (Fig. 11b; cf. Fig. 5). The bulk geometry of the ramparts is constrained by the resistance to frictional sliding on basal and internal shear planes, at rapidly decreasing strain rates before the ultimate freezing point of the Bingham fluid is reached. Although a rampart is not morphologically preserved at the Chicxulub ejecta blanket due to erosion of the upper parts, we think that the stacking of glide planes represents an interior expression of terrestrial ramparts.

CONCLUSION

Craters on both Mars and Earth were formed in the presence of an atmosphere and volatiles. This makes comparative studies very important. Because of their pristine preservation, the Ries crater in Germany and the Chicxulub crater in Mexico play an outstanding role for understanding Martian impact craters. This paper summary introduces the geology of the Ries crater, Germany, and the ejecta blanket of the Chicxulub crater, Mexico. Recent structural observations and results are presented and their relevance for the two distinct ejecta facies, observed around Martian craters, is tested and discussed.

The Ries crater study has shown that surface-parallel decoupling of the uppermost target layers occurs in the periphery of impact craters beneath the continuous ejecta blanket if a layered target exists. Detachment and radial outward transport of thin surface layers is caused by spallation and subsequent ejecta curtain dragging (Kenkmann and Ivanov 2005, 2006). A model is proposed that explains the formation of concentric furrows and ridges of the inner layers of fluidized ejecta blankets of Martian craters by detachment faulting underneath the ejecta.

The Chicxulub ejecta blanket, preserved to a previously unknown degree and proved by the occurrence of shocked quartz grains, can be traced from 3.0–5.0 radii distance and fills a karstified paleorelief. The long runout distance makes it an ideal analog to fluidized ejecta blankets of Martian impact craters. Comparative fabric analyses within the ejecta blanket indicate a transition from a noncohesive, turbulent flow to a more cohesive flow that was affected by topography towards the distal parts of the ejecta blanket. Internal shear planes become frequent. A similar gradient is observed in profiles

from the top to the bottom of the ejecta. We propose that the formation of ramparts in fluidized ejecta blankets results from a stacking of cohesive ejecta sheets bounded by internal glide planes. This most likely occurs at decreasing flow rate and shear stress when the critical yield stress of the ejecta material is reached.

Acknowledgments—T. K. would like to thank the organizers of the workshop for their kind invitation and generous travel support. The analysis of the Ries crater was done in cooperation with B. A. Ivanov (Russian Academy of Sciences) and benefited from discussions with R. Hüttner, J. Pohl, W. von Engelhardt, and D. Stöffler. We acknowledge help from D. Reiss, DLR Berlin, with preparation of MOLA profiles. The authors are grateful to Adriana C. Ocampo, Kevin O. Pope, David King, Jr., O. Barnouin-Jha, and F. Hörz for fruitful discussions on the Chicxulub ejecta. F. S. would like to express his acknowledgement to R. Tagle, L. Hecht, C. Shaw, and A. Pereira Corona for their field assistance. We thank H. Newsom for his constructive review. Research on the ejecta blanket of the Chicxulub crater was funded by the graduate research program “Faunal turnovers and mass extinctions” of the German Science Foundation at the Museum of Natural History (DFG, Grako 503, Project A1). Field work in Mexico was supported by a research grant of the Barringer Crater Company.

Editorial Handling—Dr. Nadine Barlow

REFERENCES

- Alvarez M. 1957. Exploración geologica preliminar del Rio Hondo, Quintana Roo. *Boletín de la Asociación Mexicana de Geólogos Petroleros* 6:207–213.
- Angenheister G. and Pohl J. 1969. Die seismischen Messungen im Ries von 1948–1969. *Geologica Bavarica* 61:304–326.
- Barlow N. G. 2005. Review of Martian impact crater ejecta structures and their implications for target properties. In *Large meteorite impacts III*, edited by Kenkmann T., Hörz F., and Deutsch A. Boulder, Colorado: Geological Society America. pp. 433–442.
- Barlow N. G. and Bradley T. L. 1990. Martian impact craters: Correlations of ejecta and interior morphologies with diameter, latitude, and terrain. *Icarus* 87:156–179.
- Barlow N. G., Boyce J. M., Costard F. M., Craddock R. A., Garvin J. B., Sakimoto S. E. H., Kuzmin K. O., Roddy D. J., and Soderblom L. A. 2000. Standardizing the nomenclature of Martian impact crater ejecta morphologies. *Journal of Geophysical Research* 105:26,733–26,738.
- Barnouin-Jha O. S. and Schultz P. H. 1996. Ejecta entrainment by impact-generated ring vortices: Theory and experiment. *Journal of Geophysical Research* 101:21,099–21,115.
- Barnouin-Jha O. S. and Schultz P. H. 1998. Lobateness of impact ejecta deposits from atmospheric interactions. *Journal of Geophysical Research* 103:25,739–25,756.
- Boyce J. M. and Mouginis-Mark P. J. 2005. Martian craters viewed by the THEMIS instrument: Double-layered ejecta craters (abstract). Workshop on the Role of Volatiles and Atmospheres on Martian Impact Craters. LPI Contribution #1273. pp. 27–28.

- Butterlin J. 1958. Reconocimiento geológico preliminar del Territorio de Quintana Roo. *Boletín de la Asociación Mexicana de Geólogos Petroleros* 10:531–570.
- Carr M. H., Crumpler L. S., Cutts J. A., Greeley R., Guest J. E., and Masursky H. 1977. Martian impact craters and emplacement of ejecta by surface flow. *Journal of Geophysical Research* 82: 4055–4065.
- Christensen P. R., Jakosky B. M., Kieffer H. H., Malin M. C., McSween H. Y., Nealon K., Mehall G. L., Silverman S. H., Ferry S., Caplinger M., and Ravine M. 2004. The Thermal Emission Imaging System (THEMIS) for the Mars 2001 Odyssey mission. *Space Science Reviews* 110:85–130.
- Clifford S. M. 1993. A model for the hydrologic and climatic behavior of water on Mars. *Journal of Geophysical Research* 98: 10,973–11,016.
- Costard F. M. 1989. The spatial distribution of volatiles in the Martian hydro-lithosphere. *Earth, Moon, and Planets* 45:265–290.
- Esteban M. and Klappa C. F. 1983. Subaerial exposure environment. In *Carbonate depositional environments*, edited by Scholle P. A., Bebout D. G., and Moore C. H. Tulsa, Oklahoma: American Association of Petroleum Geologists. pp. 1–54.
- Fouke B. W., Zerkle A. L., Alvarez W., Pope K. O., Ocampo A. C., Wachtmann R. J., Grajales-Nishimura J. M., Claeys P., and Fischer A. G. 2002. Cathodoluminescence petrography and isotope geochemistry of K/T impact ejecta deposited 360 km from the Chicxulub crater, at Albion Island, Belize. *Sedimentology* 49:117–138.
- Gall H., Müller D., and Stöffler D. 1975. Verteilung, Eigenschaften und Entstehung der Auswurfmassen des Impaktkraters Nördlinger Ries. *Geologische Rundschau* 64:915–947.
- Garvin J. G., Sakimoto S. E. H., Frawley J. J., and Schnetzler C. 2000. North polar region craterforms on Mars: Geometric characteristics from the Mars Orbiter Laser Altimeter. *Icarus* 144:329–352.
- Graup G. 1999. Carbonate-silicate liquid immiscibility upon impact melting: Ries crater, Germany. *Meteoritics & Planetary Science* 34:425–438.
- Handin J., Hager R. V., Friedman M., and Feather J. N. 1963. Experimental deformation of sedimentary rocks under confining pressure: Pore pressure tests. *American Association of Petroleum Geologists Bulletin* 47:717–755.
- Hildebrand A. R., Penfield G. T., Kring D. A., Pilkington M., Camargo-Zanoguera A., and Jacobsen S. B. 1991. Chicxulub crater: A possible Cretaceous/Tertiary boundary impact crater on the Yucatán Peninsula, Mexico. *Geology* 19:867–871.
- Hörz F. 1982. Ejecta of the Ries crater, Germany. In *Geological implications of impacts of large asteroids and comets on the Earth*, edited by Silver L. T. and Schultz P. H. Boulder, Colorado: Geological Society of America. pp. 39–56.
- Hörz F., Ostertag R., and Rainey D. A. 1983. Bunte breccia of the Ries: Continuous deposits of large impact craters. *Reviews of Geophysics and Space Physics* 21:1667–1725.
- Hüttner R. 1969. Bunte Trümmernmassen und Suevit. *Geologica Bavarica* 61:142–200.
- Hüttner R. 1988. Zum Bau des südlichen Ries-Kraterandes. *Jahreshefte Geologisches Landesamt Baden-Württemberg* 30: 231–251.
- Hüttner R., Brost E., Homilius J., and Schmidt-Kaler H. 1980. Struktur des Ries-Kraterandes auf Grund geoelektrischer Tiefensondierungen. *Geologisches Jahrbuch* E19:95–117.
- INEGI 1987. Carta Geológica 1:250000, hoja E16-4 (Chetumal). Mexico: Instituto Nacional de Estadística, Geografía e Informática.
- Isphording W. C. 1984. The clays of Yucatán, Mexico: A contrast in genesis. In *Palygorskite-sepiolite: Occurrences and uses*, edited by Singer A. and Galan E. Amsterdam: Elsevier. pp. 59–73.
- Ivanov B. A. 2005. Shock melting of permafrost on Mars: Water ice multiphase equation of state for numerical modeling and its testing (abstract #1232). 36th Lunar and Planetary Science Conference. CD-ROM.
- Ivanov B. A. and Pogoretsky A. V. 1996. Bingham parameters for fluidized ejecta spreading on Mars and Martian volatiles. 27th Lunar and Planetary Science Conference. pp. 587–588.
- Ivanov B. A., Murray B. C., and Yen A. S. 1994. Dynamics of fluidized ejecta blankets on Mars. 25th Lunar and Planetary Science Conference. pp. 599–600.
- Ivanov B. A., Pogoretsky A. V., and Murray B. 1997. Fluidized ejecta blankets on Mars: Estimate of material properties (abstract #1470). 28th Lunar and Planetary Science Conference. CD-ROM.
- Ivanov B. A., Artemieva N. A., and Pierazzo E. 2005. Impact cratering and material models: Subsurface volatiles on Mars (abstract). Workshop on the Role of Volatiles and Atmospheres on Martian Impact Craters. LPI Contribution #1273. pp. 55–56.
- Jakosky B. M. and Phillips R. J. 2001. Mars' volatile and climate history. *Nature* 412:237–244.
- Kahle H. G. 1969. Abschätzung der Störungsmasse im Nördlinger Ries. *Zeitschrift Geophysik* 35:317–345.
- Kenkmann T. and Ivanov B. A. 2005. Thin-skin delamination of target rocks around the Ries crater: The effect of spallation and ejecta drag (abstract # 1039). 36th Lunar and Planetary Science Conference. CD-ROM.
- Kenkmann T. and Ivanov B. A. 2006. Delamination around impact structures by spallation and ejecta dragging: An example from the Ries crater, Germany. *Earth and Planetary Science Letters*, doi:10.1016/j.epsl.2006.08.024.
- King D. T., Petruny L. W., Pope K. O., and Ocampo A. C. 2003. Possible modes of emplacement of coarse impactoclastic ejecta breccia from a large body impact on Earth: Chicxulub ejecta in Belize, Central America (abstract #4052). 3rd International Conference on Large Meteorite Impacts. CD-ROM.
- Kring D. A. 1995. The dimensions of the Chicxulub impact crater and impact melt sheet. *Journal of Geophysical Research* 100: 16,979–16,986.
- Laurenzi M. A., Bigazzi G., Balestrieri M. L., and Bouzka V. 2003. ⁴⁰Ar/³⁹Ar laser probe dating of the central European tektite-producing impact event. *Meteoritics & Planetary Science* 38: 887–894.
- López Ramos E. 1975. Geological summary of the Yucatán Peninsula. In *Ocean basins and margins, The Gulf of Mexico and the Caribbean*, edited by Nairn A. E. M. and Stehli F. G. pp. 257–282.
- Malin M. C., Edgett K. S., Carr M. H., Danielson G. E., Davies M. E., Hartmann W. K., Ingersoll A. P., James P. B., Masursky H., McEwen A. S., Soderblom L. A., Thomas P., Veverka J., Caplinger M. A., Ravine M. A., Soulanille T. A., and Warren J. L. 2001. MOC (Mars Orbiter Camera) wide-angle image M0906229, R1403041; R1901505. NASA Planetary Photojournal. <http://photojournal.jpl.nasa.gov/index.html>.
- Melosh H. J. 2005. The mechanics of pseudotachylite formation in impact events. In *Impact tectonics*, edited by Koeberl C. and Henkel H. Berlin, Heidelberg, New York: Springer. pp. 55–80.
- Morgan J., Warner M., Brittan J., Buffler R., Camargo A., Christeson G., Denton P., Hildebrand A., Hobbs R., Macintyre H., Mackenzies G., Maguire P., Marín L., Nakamura Y., Pilkington M., Sharpton V., Snyder D., Suarez G., and Trejo A. 1997. Size and morphology of the Chicxulub impact crater. *Nature* 390:472–476.
- Mouginis-Mark P. J. 1979. Martian fluidized ejecta morphology:

- Variations with crater size, latitude, altitude, and target material. *Journal of Geophysical Research* 84:8011–8022.
- Mouginis-Mark P. J. 1987. Water or ice in the Martian regolith? Clues from rampart craters seen at very high resolution. *Icarus* 71:268–286.
- Myroie J. E. and Carew J. L. 1995. Karst development on carbonate islands. In *Unconformities in carbonate strata—Their recognition and the significance of associated porosity*, edited by Budd D. A., Saller A. H., and Harris P. A. Tulsa, Oklahoma: American Association of Petroleum Geologists. pp. 55–76.
- Newsom H. E., Graup G., Iseri D. A., Geissman J. W., and Keil K. 1990. The formation of the Ries crater, West Germany: Evidence of atmospheric interactions during a larger cratering event. In *Global catastrophes in Earth history; An interdisciplinary conference on impact, volcanism and mass mortality*, edited by Sharpton V. L. and Ward P. D. Boulder, Colorado: Geological Society of America. pp. 195–206.
- Oberbeck V. R. 1975. The role of ballistic erosion and sedimentation in lunar stratigraphy. *Reviews in Geophysics and Space Physics* 13:337–362.
- Ocampo A. R., Pope K. O., and Fischer A. G. 1996. Ejecta blanket deposits of the Chicxulub crater from Albion Island, Belize. In *The Cretaceous-Tertiary event and other catastrophes in Earth history*, edited by Ryder G., Fastovsky D., and Gartner S. Boulder, Colorado: Geological Society of America. pp. 75–88.
- Ocampo A. C., Pope K. O., and Fischer A. G. 1997. Carbonate ejecta from the Chicxulub crater: Evidence for ablation and particle interaction under high temperatures and pressures (abstract #1861). 28th Lunar and Planetary Science Conference. CD-ROM.
- Osinski G. R. 2004. Impact melt rocks from the Ries structure, Germany: An origin as impact melt flows? *Earth and Planetary Science Letters* 226:529–543.
- Osinski G. R., Grieve R. A. F., and Spray J. G. 2004. The nature of the groundmass of surficial suevite from the Ries impact structure, Germany, and constraints on its origin. *Meteoritics & Planetary Science* 39:1655–1683.
- Pohl J., Stöffler D., Gall H., and Ernstson K. 1977. The Ries impact crater. In *Impact and explosion cratering*, edited by Roddy D. J., Pepin R. O., and Merrill R. B. New York: Pergamon Press. pp. 343–404.
- Pope K. O. and Ocampo A. C. 1999. The Chicxulub continuous ejecta blanket and its implications for fluidized ejecta blankets on Mars (abstract #1380). 30th Lunar and Planetary Science Conference. CD-ROM.
- Pope K. O. and Ocampo A. C. 2000. Chicxulub high-altitude ballistic ejecta from central Belize (abstract #1419). 31th Lunar and Planetary Science Conference. CD-ROM.
- Pope K. O., Ocampo A. C., and Duller C. E. 1991. Mexican site for K/T impact crater? *Nature* 351:105–108.
- Pope K. O., Ocampo A. C., Fischer A. G., Alvarez W., Fouke B. W., Webster C. L., Vega F. J., Smit J., Fritsche A. E., and Claeys P. 1999. Chicxulub impact ejecta from Albion Island, Belize. *Earth and Planetary Science Letters* 170:351–364.
- Pope K. O., Ocampo A. C., Fischer A. G., Vega F. J., Ames D. E., King D. T., Fouke B. W., Wachtman R. J., and Kletetschka G. 2005. Chicxulub impact ejecta deposits in southern Quintana Roo, Mexico, and central Belize. In *Large meteorite impacts III*, edited by Kenkmann T., Hörz F., and Deutsch A. Boulder, Colorado: Geological Society of America. pp. 171–190.
- Reiss D., van Gasselt S., Hauber E., Michael G., Jaumann R., and Neukum G. 2005. Ages and onset diameters of rampart craters in equatorial regions on Mars (abstract). Workshop on the Role of Volatiles and Atmospheres on Martian Impact Craters. LPI Contribution #1273. pp. 92–93.
- Schönián F., Kenkmann T., and Stöffler D. 2003. Internal shearing and subsurface erosion from the Chicxulub ejecta blanket (Albion Fm., Quintana Roo, Mexico) (abstract #4128). 3rd International Conference on Large Meteorite Impacts, August 5–7, 2003, Nördlingen, Germany.
- Schönián F., Stöffler D., Kenkmann T., and Wittmann A. 2004. The fluidized Chicxulub ejecta blanket, Mexico: Implications for Mars (abstract #1848). 35th Lunar and Planetary Science Conference. CD-ROM.
- Schönián F., Tagle R., Stöffler D., and Kenkmann T. 2005. Geology of southern Quintana Roo and the Chicxulub ejecta blanket (abstract #2389). 36th Lunar and Planetary Science Conference. CD-ROM.
- Scholz C. H. 1990. *The mechanics of earthquakes and faulting*. New York: Cambridge University Press. 439 pp.
- Schultz P. H. 1992. Atmospheric effects on ejecta emplacement. *Journal of Geophysical Research* 97:11,623–11,662.
- Schultz P. H. and Gault D. E. 1979. Atmospheric effects on Martian ejecta emplacement. *Journal of Geophysical Research* 84:7669–7687.
- Shoemaker E. M. and Chao E. C. T. 1961. New evidence for the impact origin of the Ries Basin, Bavaria, Germany. *Journal of Geophysical Research* 66:3371–3378.
- Smit J. 1999. The global stratigraphy of the Cretaceous-Tertiary boundary impact ejecta. *Annual Review of Earth and Planetary Sciences* 27:75–113.
- Stewart S. T. and Ahrens T. J. 2003. Shock Hugoniot of H₂O ice. *Geophysical Research Letters* 30:1332.
- Stewart S. T., O'Keefe J. D., and Ahrens T. J. 2001. The relationship between rampart crater morphologies and the amount of subsurface ice (abstract #2092). 32nd Lunar and Planetary Science Conference. CD-ROM.
- Stöffler D. 1977. Research drilling Nördlingen 1973 (Ries): Polymict breccias, crater basement, and cratering model of the Ries impact structure. *Geologica Bavarica* 75:443–458.
- Stöffler D., Artemieva N. A., and Pierazzo E. 2002. Modeling the Ries-Steinheim impact event and the formation of moldavite strewn field. *Meteoritics & Planetary Science* 37:1893–1907.
- von Engelhardt W. 1990. Distribution, petrography, and shock metamorphism of the ejecta of the Ries crater in Germany—A review. *Tectonophysics* 171:259–273.
- von Engelhardt W., Arndt J., Fecker B., and Pankau H. G. 1995. Suevite breccia from the Ries crater, Germany: Origin, cooling history and devitrification of impact glasses. *Meteoritics* 30:279–293.
- Wagner G. H. 1964. Kleintektonische Untersuchungen im Gebiet des Nördlinger Rieses. *Geologisches Jahrbuch* 81:519–600.
- Wohletz K. H. and Sheridan M. F. 1983. Martian rampart crater ejecta: Experiments and analysis of melt-water interaction. *Icarus* 56:15–37.
- Wünnemann K., Morgan J. V., and Jödicke H. 2005. Is Ries crater typical for its size? An analysis based upon old and new geophysical data and numerical modeling. In *Large meteorite impacts III*, edited by Kenkmann T., Hörz F., and Deutsch A. Boulder, Colorado: Geological Society of America. pp. 67–83.